Isotopic effects in the angular dependence of the energy loss and angular distribution of protons and deuterons in Al foils at low energies

M. Famá, J. C. Eckardt, G. H. Lantschner, and N. R. Arista
Instituto Balseiro, Centro Atómico Bariloche, Comisión Nacional de Energía Atómica, RA-8400 Bariloche, Argentina
(Received 29 December 1999; revised manuscript received 11 April 2000; published 7 November 2000)

Energy loss and straggling has been measured for hydrogen and deuterium ions in thin solid aluminum foils in the low-energy range $E<10$ keV and in the forward direction, both as a function of the energy, and at fixed energies as a function of the observation angle. Whereas no isotopic effect in the energy loss at the forward direction was observed, significant differences appeared when observing at nonzero angles. Monte Carlo simulations and model calculations of the energy loss as a function of the observation angle using a frictional-type energy loss, taking into account the path-length enlargement, the elastic energy loss, and the foil roughness, led to an understanding of the main physical features at these energies. The observed isotopic effect at nonzero angles can be fully accounted for by differences in the foil roughness influence and in the elastic energy loss.

PACS number(s): 34.50.Bw, 34.20.Cf, 02.70.Lq

I. INTRODUCTION

When a swift ion beam traverses a thin foil, it is angularly dispersed and loses energy. In experiments with light ions of energies $E/M>100$ keV/amu, traversing thin targets, an increase of some percent can be observed when measuring the energy loss ΔE as a function of the observation angle θ [1–16]. Some factors determining this increase are the path-length enlargement and the growth of the elastic energy loss with θ, which are not important at small angles. Another factor contributing to the increase of $\Delta E(\theta)$ is the foil roughness [13,17]. However, all these factors do not explain the observed increase of the energy loss at small angles. This has led some authors [18–25] to incorporate into the study the dependence of the electronic energy loss in single atomic collisions with the scattering angle φ, usually represented as $Q_{inel}(\varphi)$.

In a recent paper [26] it was shown that at energies below 10 keV the whole angular variation from 0° to 40° of the energy loss of protons in Al and Au can be explained considering only the above-mentioned first three factors, so that in this case the angular dependence of the single scattering electronic energy loss term $Q_{inel}(\varphi)$ is too small to be observed. In order to confirm this result, measurements with two isotopes of hydrogen were performed. To evaluate the influence of the different energy-loss mechanisms and provide energy loss data for deuterons at these low energies, in this paper we present energy-loss and straggling measurements in the forward direction as a function of ion velocity, as well as energy distributions for H^+ and D^+ in Al at 4.5 and 9 keV, respectively, as a function of the observation angle. From these data the angular distributions are also extracted. Additionally, to study the incidence of foil roughness on these measurements, $\Delta E(\theta)$ determinations using foils with different roughnesses have been performed.

In order to study the incidence of the different factors on the energy loss, we have performed a Monte Carlo simulation and further model calculations based on multiple-scattering (MS) theory. A special observation angle θ_r is introduced, with the property of allowing foil-roughness-independent energy-loss measurements.

II. EXPERIMENTAL PROCEDURE

The experiments were performed using the transmission method with very thin foils ($\sim$20 nm). The beams were generated by a hot discharge low-energy accelerator with a mass selector, yielding very stable intensities, modifiable in the range of 10^{-13} and 10^{-9} A/mm^2, covering the energy range between 1 and 10 keV. The spectrometric system consisted of a rotatable 127° cylindrical electrostatic energy analyzer. The energy and angular resolutions of the analyzer were 2% and $\pm 0.58°$, respectively. A combination of a sorption pump for the preliminary vacuum and a diffusion pump with an UHV-suitable liquid-nitrogen trap maintained an oil-free high vacuum.

Self-supported targets were made by evaporation under clean vacuum conditions on a very smooth plastic substrate [27], which was subsequently dissolved. The foil thicknesses were determined by matching the proton energy-loss measurements at 9 keV to previous stopping cross-section S determinations [28], which were based on comparisons with absolute empirical values at higher energies [29]. The roughness has been determined through a simple *in situ* procedure based on measurements of the energy straggling Ω of protons transmitted through the foil as described in Appendix A, and the values agree with an atomic force microscopy analysis made on test foils. More details about the equipment can be found in Ref. [26].

The energy spectra for the different observation angles θ have been measured maintaining a constant incident number of projectiles for each value of the angle. These measurements allowed a determination of the angular distributions by integration of the individual energy spectra.

The energies of the distributions have been determined by fitting them with Gaussians and taking their central values. Given the nearly Gaussian shape of the measured distributions, the resulting values are very close (within $\sim$10 eV) to the most probable value. The differences between these val-

ues and the mean values are also small ($\sim$10–25 eV depending on the spectra, over a total energy loss of about 1400 eV). This is one of the sources of experimental uncertainties. The energy losses $\Delta E(\theta)$ are obtained by the difference between the energies of the corresponding distributions determined in the preceding way, and the incident beam energy. The figures of a previous paper [26] show the good statistics of the spectra. Using the same experimental setup, new comparative measurements for protons and deuterons have been performed in order to observe the isotopic differences.

III. MODEL CALCULATIONS

Monte Carlo and model calculations are performed with the aim of gaining a better understanding of the processes, using the possibility of variation of the physical premises of the calculus. The different aspects of these calculations are described in the following.

A. Interaction potential

The interaction potential used in the Monte Carlo (MC) calculations described below was determined by fitting the measured angular distribution with the theoretical multiple-scattering functions for different potentials, including Thomas-Fermi and Lenz-Jensen expressions. Using the Sigmund-Winterbon formalism [30], we calculated the angular distributions for r^{-n} power potentials varying the n values. In the fitting procedure the large-angle tails of the distributions were not considered because of the breakdown of the small-angle assumption required for the validity of the analytical formalism. In Appendix B we describe the formalism used in this procedure.

As shown in Ref. [26] for 9-keV protons, and as will be shown below, the r^{-2} power potential leads to an adequate fit of the angular distributions. We point out that this simple potential generates an angular distribution that for our particular colliding system and the present energy range leads to a better fit than those calculated with the classical Lenz-Jensen or Thomas-Fermi potentials. However this is not a claim for the general validity of this interaction potential for other impact-parameter ranges. The present formalism was also used to calculate the derivatives of the multiple scattering function with respect to the foil thickness, necessary for an evaluation of the foil roughness effect, as will be described below.

B. Monte Carlo simulations

Monte Carlo simulations of the energy loss as a function of the observation angle have been performed in the frame of the binary collision approximation. Two schemes for the simulation of the solid were considered: the so-called *gaseous* and *liquid* models [31]. The first model considers independent single processes, and assumes that at any time the projectiles have the same probability per time unit to be scattered, which leads to a Poisson distribution of distances between two subsequent collisions. The second model considers a constant traveled distance between collisions.

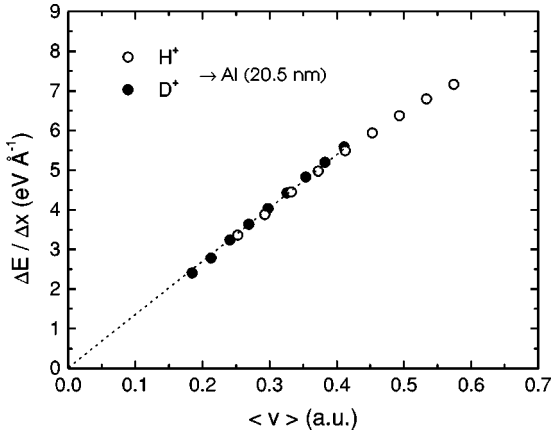

FIG. 1. Energy loss of protons and deuterons after traversing a 20.5-nm-thick Al foil in the forward direction as a function of the average projectile velocity $\langle v\rangle = 1/2(\langle v_{in}\rangle + \langle v_{out}\rangle)$. One can observe the proportionality of the energy loss with the velocity at low energies $\Delta E/\Delta x = k\langle v\rangle$, with the same constant for both isotopes.

The foil roughnesses has also been included in these calculations. In Appendix C we describe details of the simulations.

As described in Ref. [26], at the present low energies there is no evidence of the influence of an impact parameter dependence of the single collision energy losses, i.e., the $Q(\varphi)$ term. This makes the electronic energy loss $\Delta E_{elec}(\theta)$, where θ is the observation angle, directly proportional to the traveled path length. As MC calculations yield similar path lengths for the *gaseous* and *liquid* models, they yield similar $\Delta E(\theta)$ functions.

IV. RESULTS AND DISCUSSION

Figure 1 shows the projectile-velocity dependence of the forward direction energy loss of H^+ and D^+ in the very low 2–9-keV energy range, in a 20.5-nm-thick Al target. As can be observed, both isotopes yield the same values within the experimental uncertainties, confirming the smallness of the nuclear energy loss even at these low energies when considering particles emerging at zero angle. As expected, the deuterium ions show the same velocity proportionality as previously measured proton values [32], and, as predicted by theory. Figure 2 shows the energy straggling values which also are coincident within the experimental uncertainties. The depicted values are corrected for the spectrometer resolution considering Gaussian shapes. Since the measured straggling values are affected by the foil roughness [34], the observed linear dependence, with the projectile velocity in the presence of foil roughness, is a consequence of the linear dependence of both the energy loss and the straggling at these low velocities.

Figure 3 displays the angular distributions of 9-keV protons and deuterons together with normalized multiple-scattering functions calculated with Lenz-Jensen and r^{-2} potentials. Experimental points corresponding to different angles were obtained by integrating the energy spectrum taken at the corresponding angle. The theoretical values were calculated using the formalism of Ref. [30]. As already

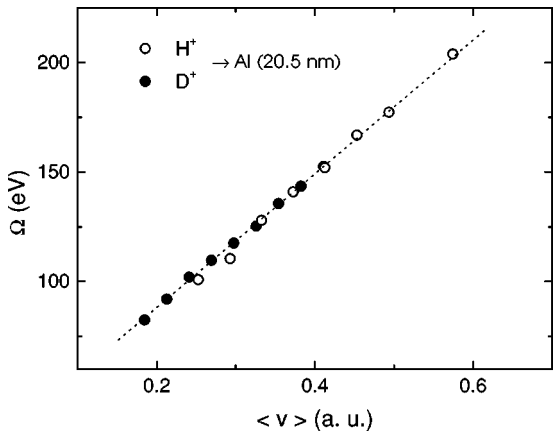

FIG. 2. Experimental energy straggling of protons and deuterons after traversing a 20.5-nm-thick Al foil in the forward direction, as a function of the projectile velocity. The dashed line is to guide the eye. The experimental values are the result of the intrinsic straggling Ω_0 and the foil roughness effect (see the text).

noted, the simple r^{-2} potential yields a better fit than the Lenz-Jensen potential, although the differences are not large. This potential, which also yields a good fit to the proton angular distributions [26], was used for the present MC calculations.

The energy loss as a function of observation angle for 4.5-keV protons and 9-keV deuterons, i.e., the same incident velocity (0.426 a.u.), after traversing a 22-nm Al foil, is shown in Fig. 4. The foil roughness of 12% was evaluated through measurements of the energy straggling and subtraction of a theoretical intrinsic energy spread, as described in Appendix A. The same roughness values were obtained through this evaluation using the data of protons and deuteron measurements.

At a first glance there is a small difference in the energy loss of the two isotopes at 0° (note that an expanded energy scale is used). However, it is not an isotopic effect. Its origin is the difference of the mean velocity of the two isotopes,

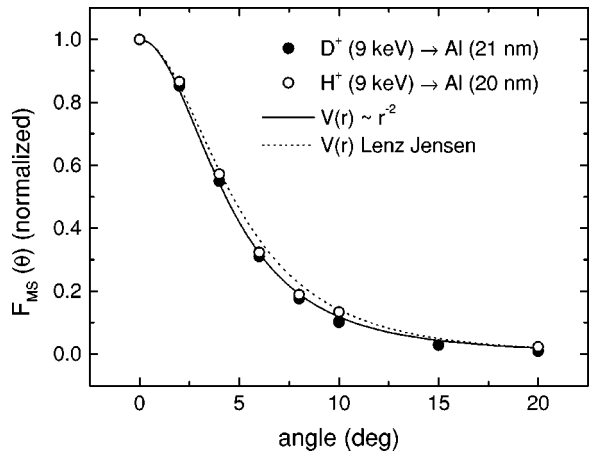

FIG. 3. Angular distribution of 9-keV deuterons in Al foils, together with the calculated distributions for the Lenz-Jensen and r^{-2} potentials (dashed and full lines, respectively). The proton data are taken from Ref. [26].

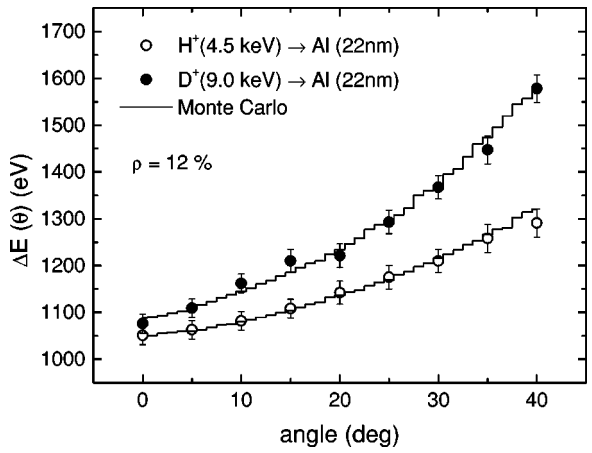

FIG. 4. Energy loss as a function of observation angle for H^+ and D^+ of the same incident velocity, together with Monte Carlo calculations. The difference at $\theta=0$ is due to differences in the mean velocity inside the foil (see text).

even though their initial velocities are the same. In particular, for the points at $\theta=0$ shown in the figure, the initial and final energies of the protons are 4500 and 3449 eV, leading to a mean velocity of 0.398 a.u., whereas for deuterons the initial and final energies are 9000 and 7924 eV, leading to a mean velocity of 0.411 a.u. Using the plot of the energy-loss data in terms of the mean velocities from Fig. 1, this leads to an energy-loss difference of $\sim$30 eV, which explains very well the experimentally observed difference. It should be stressed that this effect exists independently of the presence of an isotope effect in the energy loss. Of course this effect persists at other observation angles, and its value increase slightly with θ due to the increase of the path length, and hence of the energy loss. At the largest angle covered in this experiment, 40°, the energy-loss difference resulting using the simple $1/2[1+\sec(\theta)]$ path-length enlargement proposed in a previous paper [26] is $\simeq$35 eV. The additional difference of 5 eV with respect to the zero-angle value is very small compared to the $\Delta E_{D^+}(40°)-\Delta E_{H^+}(40°)\simeq 290$ eV variation.

As can be observed in the same figure, MC calculations lead to a very good fit of the experimental values, so we are confident that the underlying model is a good approximation of the real process. As mentioned in a previous paper [26], the calculations indicate that three main factors are responsible for the angular variation of the energy loss, namely, the increase of path length and of the nuclear energy loss with the observation angle, and the effect of foil roughness. An analytic treatment of the last factor can be found in Ref. [17]. It is shown that this effect depends on the variation of the angular distributions function with the target thickness.

The most important difference between the two isotopes arise at larger angles. It is a clear consequence of the larger elastic energy loss for the heavier isotope.

In Fig. 5 we show the experimental energy loss of deuterons as a function of observation angle in a rather rough foil, together with our MC simulations. The value of the roughness coefficient ρ is 19%, determined by the energy straggling method (Appendix A). This coefficient is defined as

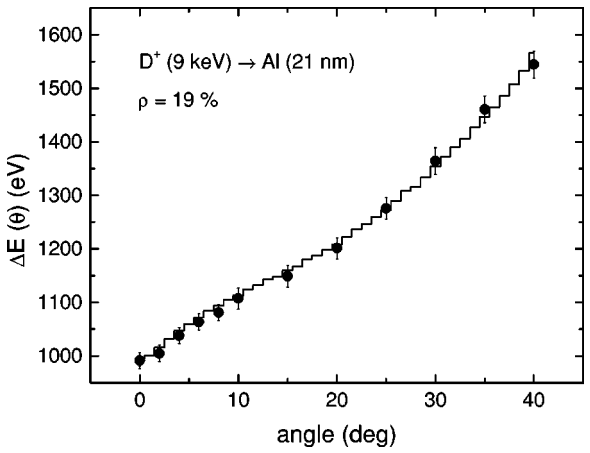

FIG. 5. $\Delta E(\theta)$ measurements and Monte Carlo calculations (step line) for 9-keV deuterons in a rather rough Al foil. The steeper increase in the range $\theta \lesssim 10°$ is essentially due to foil roughness (see text).

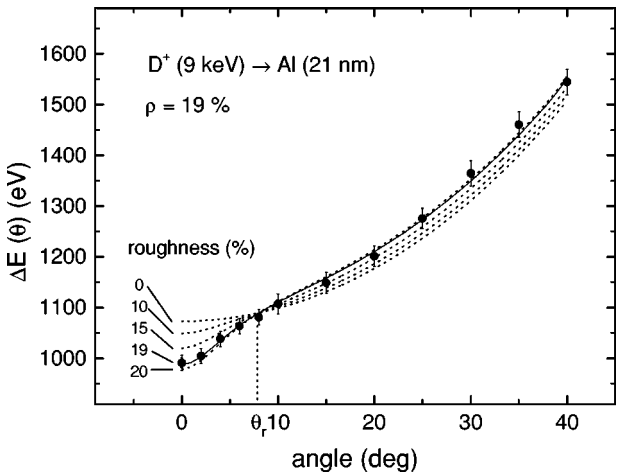

FIG. 6. Plot of the same $\Delta E(\theta)$ data of Fig. 5, together with the analytic model calculations (see the text). A good agreement up to large angles with the $\rho = 19\%$ curve can be appreciated.

$\rho \equiv \sigma_x / \langle x \rangle$, where σ_x is the previously mentioned standard deviation of the foil thickness, and $\langle x \rangle$ its mean thickness. The good fit of the MC calculations for this rough foil again indicates that the roughness effect is correctly taken into account in this simulation code. As can be observed in Fig. 5, the agreement extends up to large angles ($\theta \sim 40°$). A remarkable feature is the difference in the magnitude of the angular effect between foils of different roughnesses. Evaluating $\Delta E(\theta) - \Delta E(0)$ at $\theta = 20°$, the foil of Fig. 4 ($\rho = 12\%$) yields $\simeq 150$ eV, whereas the thinner foil with the $\rho = 19\%$ foil of Fig. 5 leads to $\simeq 213$ eV.

To evaluate the roughness effect on the angular dependence of the energy loss analytically, we use the expression resulting from the formalism given in Ref. [17]:

$$\Delta E(\theta)_{rough} \cong \overline{\Delta E}\left(1 + \rho^2 \frac{\partial \ln F(\theta,x)}{\partial \ln x}\right) = \overline{\Delta E}(1 + \rho^2 \nu(\theta)), \tag{1}$$

where the term on the left-hand side is the variation of the energy loss with the observation angle due to the foil roughness, $\overline{\Delta E}$ is the angular average of the energy loss, and $F(\theta,x)$ is the multiple-scattering function. As shown in the previously cited reference, the term $\partial \ln F(\theta,x)/\partial \ln x$ assumes negative values for small θ and positive values for larger angles; therefore, there exists an angle θ_r for which the logarithmic derivative is zero. This target-thickness-dependent angle $\theta_r(x)$ is then defined through the relation

$$\frac{\partial \ln F(\theta_r, x)}{\partial \ln x} = 0, \tag{2}$$

and has the important property that energy losses measured at this angle are free of foil roughness effects.

In Fig. 6 we show the same energy-loss measurements of Fig. 5 together with the results of the simplified model discussed in Ref. [26], synthesized by the expression

$$\Delta E(\theta) \cong \frac{\overline{\Delta E}}{2}[1 + \sec(\theta)] + \frac{4 m_1 m_2 E}{(m_1 + m_2)^2} \sin^2\left(\frac{\theta}{2}\right) + \rho^2 \nu(\theta) \overline{\Delta E}, \tag{3}$$

which includes, in addition to the foil roughness effect, the path-length enlargement in a very simplified way (first term), and approximates the nuclear energy loss in the laboratory frame by the corresponding one of the c.m. reference system (second term), in addition to neglecting the dependence of the inelastic energy loss with the impact parameter [i.e., no $Q(\varphi)$ term [26]]. This simplified model was shown to give a very good representation of the experimental results in this low-energy range.

From the previous equations one can see that the roughness term depends strongly on the value of the roughness coefficient. The figure show calculations corresponding to different ρ values. As expected, all the curves cross at the θ_r angles, which take the values of $\simeq 8°$ for the 21-nm foil. For the case of the present foil one can observe the predominance of the roughnesses term in the region $\theta \lesssim \theta_r$ (by comparison with the $\rho = 0$ curve), whereas the path-length enlargement and the increase of the nuclear energy loss dominate at larger angles [26].

The curves of the figure suggest a further way to determine foil roughnesses by measuring $\Delta E(\theta)$ in the region $0 \leqslant \theta \leqslant \theta_r$ and searching the ρ values in order to adjust the measurements. This method can be applied when the derivative $\nu(\theta)$ of the multiple-scattering function is known, and when there is a negligible influence of the angular dependence of the inelastic single collision energy loss Q_{inel} with the scattering angle, as observed at these low energies [26].

In order to check the assumptions made here, we present energy-loss measurements as a function of the observation angle in foils of different roughnesses ($\rho_1 = 8\%$ and $\rho_2 = 13\%$) and similar thicknesses ($\langle x \rangle_1 = 21$ nm and $\langle x \rangle_2 = 22$ nm), respectively. In Fig. 7 one can see the results that refer to the $\Delta E(0)$ values. From the figure it can be verified

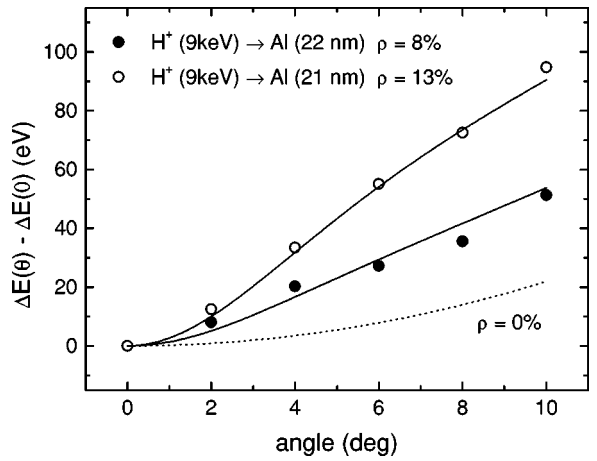

FIG. 7. $\Delta E(\theta)$ data for protons in two different Al foils referring to $\Delta E(0)$, together with the model calculations for rough foils (solid lines) and ideal smooth foil (dotted line).

that for small angles the experimental values ΔE_{expt} satisfy the relation

$$\frac{\Delta E_{\text{expt}}(\theta,\rho_2)-\Delta E_{\text{expt}}(\theta,\rho=0)}{\Delta E_{\text{expt}}(\theta,\rho_1)-\Delta E_{\text{expt}}(\theta,\rho=0)} \simeq \left(\frac{\rho_2}{\rho_1}\right)^2, \tag{4}$$

which provides an experimental support of the above described incidence of the foil roughness on these measurements.

Figure 8 shows the net isotopic effect as a function of the observation angle, and the incidence of the different contributing mechanisms. The experimental values are those of Fig. 4. Here we display the magnitude of the energy-loss difference that refers to the $\theta=0$ values, $\delta(\Delta E(\theta))-\delta(\Delta E(0))=(\Delta E(\theta)_{D^+}-\Delta E(\theta)_{H^+})-(\Delta E(0)_{D^+}-\Delta E(0)_{H^+})$. As may be observed, the main effect at large angles is due to the difference in the elastic energy loss, whereas at small angles

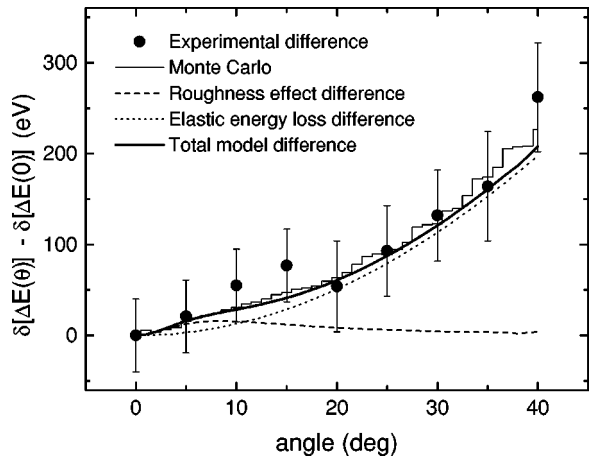

FIG. 8. Net isotopic effect on the energy loss between protons and deuterons with the same incident velocity, as a function of the observation angle, $\delta(\Delta E(\theta))-\delta(\Delta E(0))=(\Delta E(\theta)_{D^+}-\Delta E(\theta)_{H^+})-(\Delta E(0)_{D^+}-\Delta E(0)_{H^+})$. The experimental points are calculated from those of Fig. 4. The different terms of the model calculation [Eq. (3)] are plotted separately.

the largest factor is the difference of roughness effects between both isotopes due to differences in their multiple-scattering functions. This latter contribution reduces to zero at larger angles due to the same constant asymptotic value of the roughness effect at large angles. As the path-length enlargements are the same for both isotopes (within the frame of the simple model [26]), there is a negligibly small effect ($\sim$5 eV) due to the isotopic differences in the mean velocities and path-length enlargments.

V. CONCLUDING REMARKS

Energy-loss measurements with H^+ and D^+ in Al at very low energies and zero angle have been made, as well as determinations of energy and angular distributions as a function of the exit angle between 0° and 40°. Related model calculations and Monte Carlo simulations have been performed in order to obtain a better insight of the processes. From the preceding, we conclude the following.

(1) As previously found for protons [26], the observed angular dependence of the energy loss of deuterons at the present low energies can be fully explained in terms of path-length enlargement, increasing elastic energy loss and foil roughness effects.

(2) Energy loss and straggling measurements of equal velocity protons and deuterons in the forward direction yield the same values within experimental uncertainties, thus showing the absence of an isotopic effect and the smallness of the elastic energy loss mechanism when observing in the forward direction.

(3) With increasing observation angles, an increasing isotopic effect is observed. The main contribution to this feature at small angles is the foil roughness effect, whereas at larger angles it is due to increasing elastic-energy-loss differences, as follows from the model calculations of Ref. [26].

(4) The multiple-scattering calculations with a fitted r^{-2} power potential using the formalism given in Ref. [30] lead in the present energy range to a better fit of measured angular distributions than those corresponding to Thomas-Fermi and Lenz-Jensen potentials. This holds for protons as well as for deuterons.

ACKNOWLEDGMENTS

This work was supported in part by the Argentine Consejo Nacional de Investigaciones Científicas y Técnicas (Project No. PIP 4267) and the Agencia Nacional de Promoción Científica y Tecnológica (Project No. PICT0355). One of us, M.F., thanks the FOMEC program for financial support.

APPENDIX A: FOIL ROUGHNESS

The foil roughness can be estimated by means of the measured energy straggling Ω, the energy loss ΔE, and the theoretic value Ω_0 for the energy straggling corresponding to

uniform foils (intrinsic energy straggling). For a Gaussian foil thickness distribution, the experimental energy straggling can be expressed as [34]

$$\Omega^2=\Omega_0^2+\rho^2\Delta E^2, \tag{A1}$$

where the roughness coefficient ρ is defined as

$$\rho=\frac{\sigma_x}{\langle x\rangle}, \tag{A2}$$

where $\langle x\rangle$ is the average foil thickness and σ_x is the standard foil thickness deviation. Then from Eq. (A1)

$$\rho=\frac{1}{\Delta E}\sqrt{\Omega^2-\Omega_0^2}. \tag{A3}$$

For the values of Ω_0 we chose a theoretical value appropriate for low energies, obtained from density-functional calculations [33], which gives good agreement with experimental values of the first momentum (mean energy).

APPENDIX B: MULTIPLE-SCATTERING FUNCTION

In order to calculate the angular distributions for different potentials, we followed the formalism developed in Ref. [30]. The scaled angular distribution of a particle beam after traversing a thin layer of material is given by

$$f_1(\tau,\tilde{\alpha})=\int_0^\infty z dz J_0(\tilde{\alpha}z)\exp[-\tau\Delta(z)] \tag{B1}$$

in terms of the foil thickness and observation angles measured in reduced units, namely,

$$\tau=\pi a^2 N x,\quad \tilde{\alpha}=\frac{Ea}{2Z_1Z_2e^2}\alpha, \tag{B2}$$

where x is the penetrated depth, α is the observation angle, $a=0.8853a_0/(Z_1^{2/3}+Z_2^{2/3})^{1/2}$ is the screening radius, N is the atomic density, E is the ion energy, Z_1 and Z_2 is the atomic numbers of the ion and target respectively, and e is the elementary charge. In Eq. (B1) J_0 is the zero-order Bessel function of the first kind, z is an integration variable, and

$$\Delta(z)=\int_0^\infty d\tilde{\varphi}\,\frac{f(\tilde{\varphi})}{\tilde{\varphi}^2}[1-J_0(z\tilde{\varphi})], \tag{B3}$$

where $f(\tilde{\varphi})$ is a the scattering function describing the differential cross section of the single scattering events, and thus is a functional of the potential.

For a power potential, $V(r)\propto r^{-n}$, the scattering function is given by $f(\tilde{\varphi})=\lambda\tilde{\varphi}^{1-2/n}$ [35]. For this potential one obtains

$$\Delta(z)=cz^{2/n},\quad c=-\frac{\lambda\Gamma(-1/n)}{2^{2/n+1}\Gamma(1+1/n)} \tag{B4}$$

which by integration of Eq. (B1) yields the multiple-scattering function.

APPENDIX C: MONTE CARLO

Following is a description of the main ingredients of the Monte Carlo simulation procedure.

1. Polar scattering angle

Following references [36,37], we sort the c.m. scattering angle by means of a random number k_a, using scattering cross sections in terms of reduced units. In order to do so we recall that the reduced differential scattering cross section $dJ/d\tilde{\varphi}$ is related to the scattering function $f(\tilde{\varphi})$ through the relation [35]

$$\frac{dJ}{d\tilde{\varphi}}=\frac{f(\tilde{\varphi})}{\tilde{\varphi}^2}, \tag{C1}$$

with $\tilde{\varphi}=\varepsilon\sin(\varphi/2)$, where $\varepsilon=am_2E/Z_1Z_2(m_1+m_2)$ is the reduced energy.

Integrating the right term of Eq. (C1), one obtains the reduced scattering cross section $J(\tilde{\varphi})$ which satisfies the condition

$$J_{tot}=\int_{\tilde{\varphi}_{\min}}^{\varepsilon}\frac{f(\tilde{\varphi}^*)}{\tilde{\varphi}^{*2}}d\tilde{\varphi}^*=J(\varepsilon)-J(\tilde{\varphi}_{\min}), \tag{C2}$$

where $J_{tot}=(r_0/a)^2$, with $r_0=\frac{1}{2}N^{-1/3}$, a is the screening radius, and ε is the reduced energy [36,37].

The normalized random quantity is

$$\frac{[J(\tilde{\varphi})-J(\varphi_{\min})]}{J_{tot}}, \tag{C3}$$

which can be generated by a random number k_a between 0 and 1. Therefore, for a power potential $V(r)\sim r^{-n}$, which leads to a scattering function $f(\tilde{\varphi})=\lambda_n\tilde{\varphi}^{1-2/n}$, it is possible to sort out the reduced angle $\tilde{\varphi}$ through the equation

$$\tilde{\varphi}=\left[\frac{2}{n\lambda_n}J_{tot}^2k_a+\varepsilon^{-2/n}\right]^{-n/2}, \tag{C4}$$

where the constant λ_n is taken from Ref. [35].

For $n=2$ this expression takes the form

$$\tilde{\varphi}=\left[\frac{1}{0.326}J_{tot}^2k_a+\varepsilon^{-1}\right]^{-1}. \tag{C5}$$

2. Azimuthal angle

Due to the azimuthal symmetry of the scattering process, the azimuthal angle ψ can be simply sorted through a random number k_b between 0 and 1, with

$$\psi = 2\pi k_b . \tag{C6}$$

3. Distance between collisions

We use two frequently employed models for the distances between two subsequent collisions in solids: the so-called *gaseous* and *liquid* models [31].

a. Gaseous model

The basis of this model is the assumption that at any time there is the same collision probability, irrespective of the previous history. This leads to the following relation between the distance λ between collisions and a random number k_c, satisfying $0 < k_c \leq 1$:

$$\lambda = \frac{1}{NJ_{tot}} \ln k_c , \tag{C7}$$

where N is the atomic density.

b. Liquid model

In this model a constant distance between collisions, $\lambda = \lambda_0$, with $\lambda_0 = 0.5N^{-1/3}$, is simply assumed.

4. Energy loss

To evaluate the energy loss corresponding to each collision, we calculate the electronic or inelastic component, considering it proportional to the traveled path λ between collisions

$$\Delta E_{elec} = \lambda S_e(E), \tag{C8}$$

where $S_e(E)$ is the instantaneous stopping power.

The nuclear or elastic component for each collision can be written in terms of the c.m. single scattering angle φ as

$$\Delta E_{nucl} = \frac{4m_1 m_2 E}{(m_1 + m_2)^2} \sin^2(\varphi/2). \tag{C9}$$

5. Foil roughness

The MC calculations take into account the foil roughness, considering projected path-length distributions with the same standard thickness deviation σ_x than those of the real foils. In our case, Gaussian distributions are considered. However, we have verified that the results are insensitive to the shape of the distributions whenever equivalent σ_x values are taken.

[1] G. A. Iferov and Yu. N. Zhukova, Phys. Status Solidi B **110**, 653 (1982).

[2] G. A. Iferov, V. A. Khodyrev, E. I. Sirotinin, and Yu. N. Zhukova, Phys. Lett. **97A**, 283 (1983).

[3] R. Ishiwari, N. Shiomi, and N. Sakamoto, Phys. Rev. A **25**, 2524 (1982).

[4] R. Ishiwari, N. Shiomi, and N. Sakamoto, Phys. Rev. A **30**, 82 (1984).

[5] R. Ishiwari, N. Shiomi, N. Sakamoto, and H. Ogawa, Nucl. Instrum. Methods Phys. Res. B **13**, 111 (1986).

[6] R. Ishiwari, N. Shiomi-Tsuda, N. Sakamoto, and H. Ogawa, Nucl. Instrum. Methods Phys. Res. B **48**, 65 (1990).

[7] R. Ishiwari, N. Shiomi-Tsuda, N. Sakamoto, and H. Ogawa, Nucl. Instrum. Methods Phys. Res. B **51**, 209 (1990).

[8] N. Sakamoto, N. Shiomi, and R. Ishiwari, Phys. Rev. A **27**, 810 (1983).

[9] N. Sakamoto, H. Ogawa, N. Shiomi-Tsuda, and R. Ishiwari, Nucl. Instrum. Methods Phys. Res. B **69**, 84 (1992).

[10] H. Geissel, W. N. Lennard, H. R. Andrews, D. P. Jackson, I. V. Mitchell, D. Philips, and D. Ward, Nucl. Instrum. Methods Phys. Res. B **12**, 38 (1985).

[11] H. Geissel, K. B. Winterbon, and W. N. Lennard, Nucl. Instrum. Methods Phys. Res. B **27**, 333 (1987).

[12] W. M. Arnoldbik, V. A. Khodyrev, G. A. Iferov, and D. O. Boerma, Nucl. Instrum. Methods Phys. Res. B **136**, 91 (1998).

[13] P. Mertens and Th. Krist, Nucl. Instrum. Methods Phys. Res. B **13**, 95 (1986).

[14] J. C. Eckardt, G. H. Lantschner, M. M. Jakas, and V. H. Ponce, Nucl. Instrum. Methods Phys. Res. B **2**, 168 (1984).

[15] A. A. Bednyakov, V. Ya. Chumanov, O. V. Chumanova, G. A. Iferov, V. A. Khodyrev, A. F. Tulinov, and Yu. N. Zhukova, Nucl. Instrum. Methods Phys. Res. B **13**, 146 (1986).

[16] A. A. Bednyakov, V. Ya. Chumanov, O. V. Chumanova, G. A. Iferov, V. S. Kulikauskas, I. I. Rasgulyaev, and Yu. N. Zhukova, Nucl. Instrum. Methods Phys. Res. B **115**, 168 (1996).

[17] M. M. Jakas and N. E. Capuj, Nucl. Instrum. Methods Phys. Res. B **36**, 491 (1989).

[18] A. Gras-Martí, Nucl. Instrum. Methods Phys. Res. B **9**, 1 (1985).

[19] N. M. Kabachnik, V. N. Kondratev, and O. V. Chumanova, Phys. Status Solidi B **145**, 103 (1988).

[20] T. Kaneko, Surf. Sci. **236**, 203 (1990).

[21] E. H. Mortensen, H. H. Mikkelsen, and P. Sigmund, Nucl. Instrum. Methods Phys. Res. B **61**, 139 (1991).

[22] I. S. Tilinin, Nucl. Instrum. Methods Phys. Res. B **115**, 102 (1996).

[23] H. Ascolani and N. R. Arista, Phys. Rev. A **33**, 2352 (1986).

[24] P. L. Grande and G. Schiwietz, Phys. Rev. A **44**, 2984 (1991).

[25] Yueyuan Xia, Chunyu Tan, and W. N. Lennard, Nucl. Instrum. Methods Phys. Res. B **90**, 41 (1994).

[26] M. Famá, G. H. Lantschner, J. C. Eckardt, C. D. Denton, and N. R. Arista, Nucl. Instrum. Methods Phys. Res. B **164-165**, 241 (2000).

[27] A. Valenzuela and J. C. Eckardt, Rev. Sci. Instrum. **42**, 127 (1971).

[28] J. E. Valdés, G. Martínez-Tamayo, G. H. Lantschner, J. C. Eckardt, and N. R. Arista, Nucl. Instrum. Methods Phys. Res. **73**, 313 (1993).

[29] J. F. Ziegler and J. Biersack, *The Stopping and Range of Ions in Solids* (Pergamon, New York, 1985), Vol. 1; the stopping cross sections were calculated using the STOP program from TRIM-90 with the coefficients from the file SCOEF-88.

[30] P. Sigmund and K. B. Winterbon, Nucl. Instrum. Methods **119**, 541 (1974).
[31] W. Eckstein, *Computer Simulation of Ion-Solid Interaction* (Springer, New York, 1991).
[32] G. Martínez-Tamayo, J. C. Eckardt, G. H. Lantschner, and N. R. Arista, Phys. Rev. A **54**, 3131 (1996).
[33] I. Nagy, A. Arnau, and P. M. Echenique, Phys. Rev. A **40**, 987 (1989).
[34] F. Besenbacher, J. U. Andersen, and E. Bonderup, Nucl. Instrum. Methods **168**, 1 (1980).
[35] J. Lindhard, V. Nielsen, and M. Scharff, Mat. Fys. Medd. K. Dan. Vidensk. Selsk. **36**, 10 (1968).
[36] W. Möller, G. Pospiech, and G. Schrieder, Nucl. Instrum. Methods **130**, 265 (1975).
[37] D. Zajfman, G. Both, E. P. Kanter, and Z. Vager, Phys. Rev. A **41**, 2482 (1990).